Design of Miniaturized Substrate Integrated Filters Using Aggressive Space Mapping

Jorge D. Martínez*, Stefano Sirci‡ and Vicente E. Boria‡
*I3M, Universitat Politècnica de València, València, Spain
‡iTEAM, Universitat Politècnica de València, València, Spain

***Abstract*—An optimization procedure for the design of miniaturized substrate integrated quasi-lumped filters based on aggressive space mapping techniques is presented in this paper. A gradient-descent approach based on a lossy coarse model is employed. Thus, a $3-$pole bandpass filter response centered at 10 GHz is designed, manufactured and measured, showing the validity of the technique even if strong dependencies between the different electrical and physical parameters are present.**

I. Introduction

Lumped and quasi-lumped element filters present the advantage of wider bandwidth and smaller size compared to distributed-element implementations [1], [2], usually at the expense of slightly higher losses. Particularly, they are extremely useful when a miniaturized implementation is required (e.g. surface-mounted packaged filters or switched-filter banks for multi-band application).

Recently, a quasi-lumped implementation of substrate integrated filters was proposed [3], having the advantage of a huge size reduction compared to conventional substrate integrated waveguide (SIW) filters. However, even if the proposed design procedure could benefit from an optimization approach based on parameter extraction from a fine model evaluation, no systematic optimization approach enabling the automated design of such filters was presented.

In this paper, an optimization method based on aggressive space mapping (ASM) techniques [4] is proposed for the design of substrate integrated quasi-lumped element filters. In this approach, losses are introduced in the coarse model for improving the parameter extraction (PE) process. Additionally, a gradient-descent approach [5], based on keeping a constant Jacobian matrix through the whole optimization process, is followed in order to overcome the limited accuracy of the PE process. For demonstrating the proposed approach, a miniaturized $3-$pole bandpass filter at 10 GHz is designed and optimized, showing a good agreement between simulated and measured results.

II. Filter Structure

The proposed substrate integrated quasi-lumped filters were already presented in [3]. A single resonator consists on a plated via hole of diameter d_v connected to the bottom ground plane, while ending on a rectangular metal patch $l_p \times w_p$ at the top layer. This metal patch provides a capacitive loading to the top ground plane by means of an isolating gap g_f. The whole resonator can be embedded into an SIW section of width W in order to shield the structure. A scheme of the proposed topology is shown in Fig. 1.

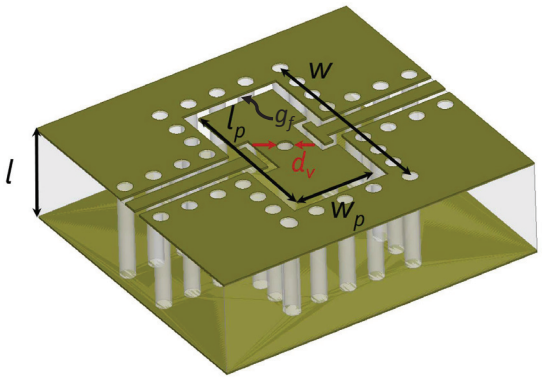

Fig. 1. Structure of the substrate integrated quasi-lumped resonator.

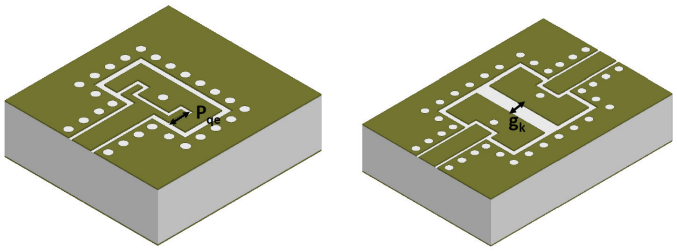

Fig. 2. (a) Input/output and (b) inter-resonator coupling schemes based on capacitive probe penetration p_{qe} and distance between resonators g_k.

The former structure can be easily modeled as a lumped-element parallel RLC resonator in shunt configuration, where the value of each element would be

$$L_r = \frac{\eta_0 l}{2\pi c_0} \ln\left(\frac{4W}{\pi d_v}\right) \tag{1}$$

$$C_r = \frac{1}{\omega_0^2 L_r} \tag{2}$$

$$R_r = \omega_0 L_r Q_0 \tag{3}$$

where η_0 is the wave impedance of free space, c_0 the speed of light in vacuum, w_0 the resonant frequency and Q_0 the unloaded Q-factor of the resonator.

Several of these resonators can be cascaded in order to implement a filter. The input/output coupling is provided by the penetration p_{qe} of a capacitive probe into the rectangular patch, while the inter-resonator coupling can be controlled by the distance g_k between adjacent resonators. A scheme of both approaches is shown in Fig. 2.

A. Design procedure

Firstly, the lumped-element equivalent circuit of the filter based on inverter-coupled resonators must be obtained using a classical synthesis procedure for in-line bandpass filters:

1) The low-pass prototype coefficients g_i are computed from the desired response.
2) The resonator is initially dimensioned (i.e. concretely d_v and W) according to the desired level of inductance. This must be a trade-off between manufacturing tolerances and degree of miniaturization. Then, the element values of the RLC parallel resonator are obtained from (1)-(3).
3) The inverter values are computed from the well-known expressions [6]

$$J_{0,1} = J_{n,n+1} = \sqrt{\frac{Y_0 \text{FBW} \omega_0 C_r}{g_0 g_1}} \tag{4}$$

$$J_{i,i+1} = \text{FBW} \omega_0 C_r \sqrt{\frac{1}{g_i g_{i+1}}} \tag{5}$$

Once the equivalent circuit has been developed, design curves relating electrical and physical parameters are required. In order to do this, three main elements must be considered: resonant frequency ω_0 as a function of the capacitive gap g_f, external Q-factor Q_{ext} versus capacitive probe penetration p_{qe}, and inter-resonator coupling coefficient k_{ij} versus resonator spacing g_k.

The input/output and middle resonator cases must be separately studied, due to the strong disturbance introduced by the input/output capacitive probe. Moreover, the Q_{ext} and k_{ij} can be related to the corresponding inverter values as $Q_{\text{ext}} = \frac{Y_0 \omega_0 C_r}{J_{0,1}^2}$ and $k_{ij} = \frac{J_{i,j}}{\omega_0 C_r}$ respectively.

The procedure for obtaining these curves from EM simulations follows the standard approach described in [6], [7]. Lastly, an initial layout of the filter can be established by obtaining the required physical parameters from the design curves for each element of the equivalent circuit. However, this initial point is typically far from the desired response, requiring extensive optimization in order to match the design specifications.

III. Optimization

Given the initial response, an optimization procedure can be applied in order to reduce the time and computational effort required for recovering the desired response. The optimization procedure proposed in this work follows a standard ASM approach, and the algorithm flow is described in Fig. 3. One evaluation of the fine model is perfomed at each iteration.

1: **procedure** OPTIMIZATION($\mathbf{x_c^*}$)
2: Compute $\mathbf{B}$ and $\mathbf{x_f}^{(0)}$ from design curves
3: **repeat**
4: Fine model evaluation $R_f[\mathbf{x_f}^{(i)}]$
5: Extract $\mathbf{x_c^{(i)}}$ from $R_c[\mathbf{x_c}^{(i)}] \approx R_f[\mathbf{x_f}^{(i)}]$
6: $\Delta x_c^{(i)} \leftarrow x_c^{(i)} - x_c^*$
7: Solve $\mathbf{B} \cdot \Delta x_f^{(i+1)} = -\Delta x_c^{(i)}$
8: $x_f^{(i+1)} \leftarrow x_f^i + \Delta x_f^{i+1}$
9: **until** ($||\mathbf{\Delta x_f^{(i+1)}}|| < \epsilon$)
10: **end procedure**

Fig. 3. Description of the ASM algorithm.

Then, the PE process will provide the element values of the coarse model that minimize the error between the S-parameters at both spaces.

Thus, the process starts from the optimized coarse model producing the desired response $\mathbf{x_c^*}$. Then, an initialization step is performed by computing the initial point of the fine model $\mathbf{x_f}^{(0)}$ and the Jacobian matrix $\mathbf{B}$ from the design curves. These curves f_i relate each electrical parameter of the coarse electrical model with its corresponding physical parameter of the fine EM model

$$f_i : x_{f,i} \rightarrow x_{c,i} \tag{6}$$

In order to obtain these curves, segmentation can be applied as it has been discussed in Section II.

The matrix $\mathbf{B}$ can be obtained as an approximation of the Jacobian matrix given by

$$\mathbf{B} = \begin{pmatrix} \frac{\partial x_{c,1}}{\partial x_{f,1}} & 0 & \cdots & 0 \\ 0 & \frac{\partial x_{c,2}}{\partial x_{f,2}} & \cdots & 0 \\ \vdots & \vdots & \ddots & 0 \\ 0 & 0 & \cdots & \frac{\partial x_{c,n}}{\partial x_{f,n}} \end{pmatrix} \tag{7}$$

Note that $\mathbf{B}$ will not be updated after each iteration, following in this case a gradient-descent approach that enables us to cope with the limited accuracy of the PE process and the simple coarse model employed. Of course, this will be at expense of an increased number of iterations in order to reach convergence.

The optimization loop is stopped when the magnitude of the displacement vector in the fine model space $||\mathbf{\Delta x_f}^{(i+1)}||$ falls below a predefined convergence goal ϵ at a given step i.

IV. Design Example

In order to demonstrate the validity of the proposed approach, a $3-$pole bandpass filter with Chebyshev response has been designed at 10 GHz with 7% FBW and 15 dB of minimum in-band return loss. The filter will be implemented in a 1.524 mm-thick substrate with $\epsilon = 3.55$ and $\tan\delta = 2.7{\cdot}10^{-3}$.

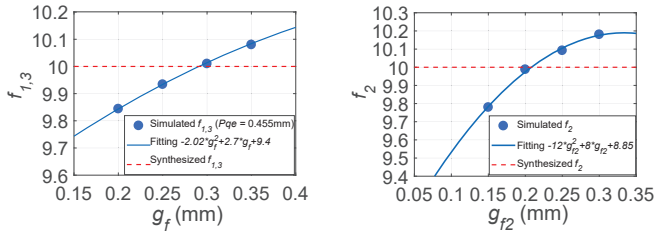

(a) (b)

Fig. 4. (a) Resonant frequency of the first/last resonator as a function of the gap g_f, and (b) resonant frequency of the second resonator as a function of the gap g_{f2}.

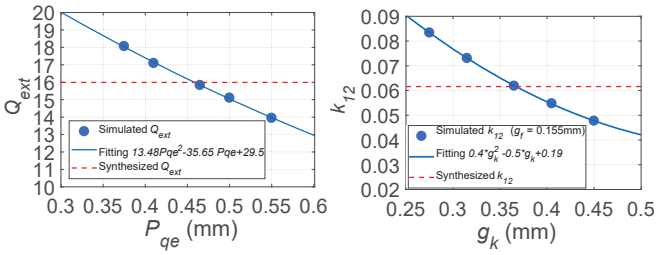

(a) (b)

Fig. 5. (a) External quality factor Q_{ext} as a function of the capacitive probe penetration p_{qe}, and (b) coupling coefficient between resonators $1-2$ and $2-3$ as a function of the spacing g_k.

A. Coarse Model and Initial Layout

Firstly, the low-pass prototype coefficients can be computed from the desired response as $g_0 = g_4 = 1$, $g_1 = g_3 = 1.119$ and $g_2 = 1.154$. Then, the inverter values can be obtained from (4)-(5), thus providing $J_{0,1} = J_{3_4} = 0.00473$ and $J_{1,2} = J_{2,3} = 0.0011$.

The level of inductance is set to $L_r = 0.892$ nH, which corresponds to a via diameter $d_v = 0.25$ mm and an SIW cavity width $W = 3.67$ mm. Therefore, the required level of capacitance will be $C_r = \frac{1}{\omega_0^2 L_r} = 0.284$ pF. If we consider an estimated Q_0 of 150, the equivalent parallel resistance should be 8.4 kΩ.

Then, the optimum coarse model is given by the resonant frequencies of resonators $1-3$ and 2, as well as the required level of Q_{ext} and $k_{1,2} = k_{2,3}$. Therefore, it can be represented as a four-element vector given by $\mathbf{x_c}* = \{f_{1,3}, f_2, Q_{\text{ext}}, k_{12,23}\} = \{10, 10, 15.99, 0.0616\}$, where both frequencies are in GHz, while the remaining parameters are dimensionless.

Next, the design curves for the former structure can be obtained by studying the different sub-components of the filter: resonator $1-3$, resonator 2, external Q-factor and coupling coefficient between resonators $1-2$ and $2-3$. From a small number of EM simulations, design curves can be obtained by fitting a quadratic function to the samples of each parameter. In this case, four different curves have been obtained and they are presented in Figs. 4 and 5.

An initial point for the fine model can be interpolated from the design curves, and it can be expressed as $\mathbf{x_f^{(0)}} = \{g_f, g_{f2}, p_{\text{qe}}, g_k\} = \{0.291, 0.209, 0.459, 0.368\}$, where all dimensions are in mm.

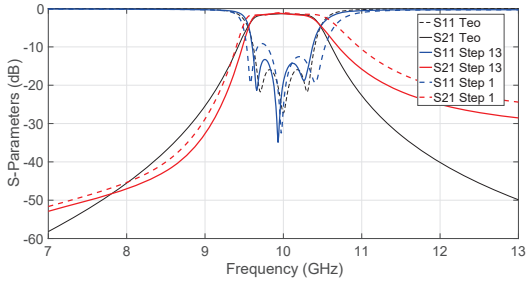

Fig. 6. Comparison between synthesized response (black), initial response at step 1, and optimized response after step 13.

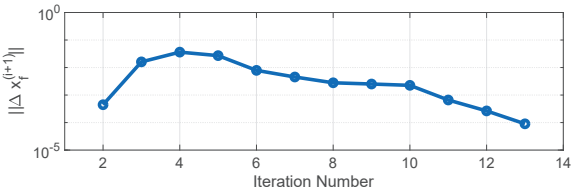

Fig. 7. Convergence of the optimization.

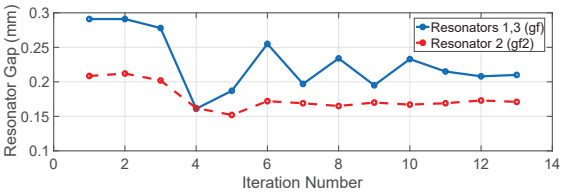

Fig. 8. Evolution of the capacitive gap for the first/third gf and second gf_2 resonators.

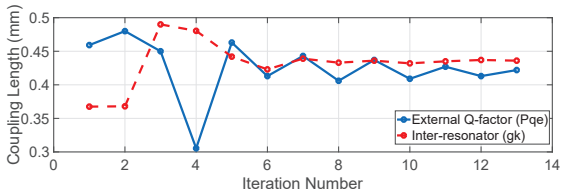

Fig. 9. Evolution of the input/output Pqe and inter-resonator gk coupling lengths.

As can be seen in Fig. 6, the initial response of the filter presents a much wider bandwidth than expected and the minimum in-band return loss specification is not satisfied.

B. Filter Optimization

In order to match the desired response given by the optimum coarse model $\mathbf{x_c^*}$, the optimization procedure is started. The coarse model is optimized using a conventional circuit simulator and a local optimization routine for parameter extraction. The evaluations of the fine model are performed using a full-wave 3D EM simulator.

TABLE I
ELEMENT VALUES OF THE COARSE MODEL

Element	Optimum	Step 13
$f_{1,3}$	10 GHz	9.998 GHz
f_2	10 GHz	9.998 GHz
Q_{ext}	15.99	16.46
$k_{12} = k_{23}$	0.06159	0.06119

TABLE II
PARAMETER VALUES OF THE FINE MODEL

Parameter (mm)	Initial	Step 13
g_f	0.291	0.210
g_{f2}	0.209	0171
p_{qe}	0.459	0.422
g_k	0.368	0.436

The Jacobian matrix $\mathbf{B}$ is computed from the derivatives of the fitted design curves at the initial point as

$$\mathbf{B} = \begin{pmatrix} 1.5374 & 0 & 0 & 0 \\ 0 & 3.0099 & 0 & 0 \\ 0 & 0 & -23.2696 & 0 \\ 0 & 0 & 0 & -0.1993 \end{pmatrix} \quad (8)$$

As shown in Fig. 7, a convergence level below $1 \cdot 10^{-4}$ is reached after 13 iterations. It is interesting to note that the first iteration presents a relatively small value of $||\mathbf{\Delta x_f}^{(2)}|| = 4.5 \cdot 10^{-4}$. This is due to the fact that the resonators were initially centered at almost the right frequency, even if the bandwidth was much higher than the specified value. Thus, the corrections at the first step were focused on the couplings, reducing the magnitude of the total change in the fine model domain. However, due to the characteristics of the filter, any change on the Q_{ext} and k_{ij} affects importantly the resonant frequency of the resonators, requiring additional corrections from this step on.

The evolution of the different variables in the fine model are shown in Figs. 8 and 9. It can be seen how greater changes are required at the first steps, while the final parameter values oscillates around the final value with decreasing corrections after each iteration. The final values of both models are summarized in Tables I and II.

V. MEASUREMENTS

The filter has been manufactured using a standard single-side PCB process. A photograph of the fabricated device can be seen in Fig. 10. Final device size is 3.74×5.45 mm^2, thus implying a huge degree of miniaturization compared to a conventional SIW or distributed planar implementation. Measured results can be seen in Fig. 11, showing a good agreement with simulations with the exception of a marginally shifted reflection zero (that produces some degradation of the minimum in-band return loss compared to the specifications). Insertion loss at center frequency is 1.87 dB, and the Q_0 was also measured in a single resonator showing a value about

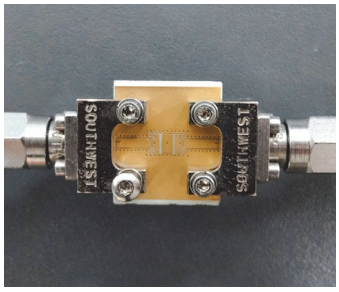

Fig. 10. Photograph of the manufactured device during measurements.

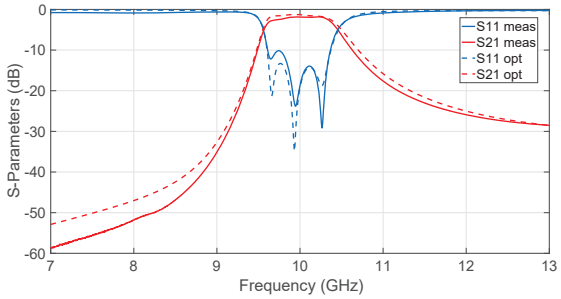

Fig. 11. Comparison between measurements and simulated results after optimization.

180. Even if this implies a small degradation compared to a conventional SIW cavity, this is mainly due to the important miniaturization of the device, that requires a footprint more than 10 times smaller than its TE_{101} SIW counterpart.

VI. CONCLUSIONS

The design and optimization of substrate integrated miniaturized filters have been demonstrated in this work. The optimization procedure is based on ASM techniques using a very simple coarse model and following a gradient-descent approach. A $3-$pole bandpass filter example has been presented, showing that a satisfactory design can be achieved with a limited number of iterations.

REFERENCES

[1] S. Qian and J. Hong, "Miniature quasi-lumped-element wideband bandpass filter at 0.5 - 2 GHz band using multilayer liquid crystal polymer technology", *IEEE Trans. Microw. Theory Tech.*, vol. 60, no. 9, pp. 2799 - 2807, Sep. 2012.

[2] Z. Ma, K. Ma, S. Mou and F. Meng, "Quasi-lumped element filter based on substrate-integrated suspended line technology", IEEE Trans. Microw. Theory Tech., vol. 65, no. 12, Dec. 2017, pp. 5154 – 5161.

[3] J.D. Martínez, H. Galindo, S. Sirci and V.E. Boria, "Miniaturized filters based on SIW quasi-lumped elements", *IEEE MTT-S Int. Conf. on Numerical Electromagnetics and Optimization*, pp. 1-4, 2018.

[4] J.E. Rayas-Sánchez, "Power in simplicity with ASM", IEEE Microwave Magazine, vol. 17, no. 4, Apr. 2016, pp. 64 – 76.

[5] J.W. Bandler, Q.S. Cheng, S.A. Dakroury, A.S. Mohamed, M.H. Bakr, K. Madsen and J. Sondergaard, "Space mapping: the state of the art", *IEEE Trans. Microw. Theory Tech.*, vol. 52, no. 1, pp. 337-361, Jan. 2004.

[6] J.S. Hong and M.J. Lancaster. *Microstrip Filters for RF/Microwave Applications*. New York, NY: John Wiley & Sons, 2001, pp. 56-61.

[7] J.B. Ness, "A unified approach to the design, measurement, and tuning of coupled-resonator filters", IEEE Trans. Microw. Theory Tech., vol. 46, no. 4, pp. 343 - 351, Apr. 1998.